THEORETICAL AND APPLIED MECHANICS
Volume 49 (2022) Issue 2, 137–155 DOI: https://doi.org/10.2298/TAM221030010R

PARAMETRICALLY EXCITED UNIDIRECTIONAL WAVE PROPAGATION IN THIN BEAM PHONONICS

Nevena Rosić, Danilo Karličić, Milan Cajić, and Mihailo Lazarević

Abstract. Wave attenuation, filtering and guiding is an ongoing topic of scientific research, as there are many opportunities for improvement of existing solutions in modern industry. One of the recent advancements has been made with the use of non-reciprocal metamaterials.Certain properties of metamaterials have made them suitable for use in various engineering fields. In this study, we investigate non-reciprocal wave propagation behavior in coupled thin beams phononics, due to time-modulation of material properties and axial loads. We compare the results for the beams which are interconnected with Winkler's type of elastic layers and elastic or viscoelastic Pasternak layers. An analytic approach is used to discover directional band gaps and investigate wave propagation through these systems of beams, at relevant excitation frequencies. The proposed framework can be exploited in further analysis of phononic systems based on multiple beams coupled through different mediums and structural elements modeled with higher-order beam theories.

1. Introduction

There is a growing demand for phononic mediums in physics and engineering. Recently developed phononic-like materials and periodic structures in their mechanical setup demonstrated interesting capabilities and wave phenomena which are not usually encountered and, as such, belong to a class of artificial materials known as metamaterials. Scientific research on this topic has spread to almost every area of engineering, from nanoscale problems to multi-span bridges [1]. Some exciting and otherwise impossible phenomena have been discovered, such as the possibility of negative mass density, moduli and Poisson's ratio [2], or non-reciprocal wave propagation. Non-reciprocity provides different opportunities for wave-steering and wave-guiding, which makes applications of phononic mediums wide and diverse [2, 4]. Also, elastic cloaking can be achieved, in which elastic waves seem to propagate as if the cloaked object does not exist and it appears to

2020 *Mathematics Subject Classification:* 74H45; 74J05; 74K10.
Key words and phrases: beam system, phononic systems, Bloch theorem, Euler–Bernoulli beam, Winkler layer, Pasternak layer, elastic, viscoelastic, periodicity, time-modulated properties, non-reciprocal wave propagation.

be invisible [2]. Acoustic metamaterials have also been successfully employed for noise cancellation, in the form of plates and membranes [2]. These metamaterials have also been tested for wave rectification and active control with piezoelectric actuators [3, 4].

As a special branch of scientific research, periodicity has been imposed to different types of structural elements (such as rods, beams, membranes, plates, etc.) and their dynamic properties have been studied under various loading and boundary conditions. Euler–Bernoulli beams have been studied extensively and it has been shown that with time modulation of material parameters dispersion branches split, but symmetry remains unbroken. However, when spatial periodicity of these properties is introduced as well, the band diagram becomes asymmetrical and so-called directional band gaps appear [5]. Non-reciprocal wave propagation has since been demonstrated in various models of structural elements with induced space-time periodic modulation [3, 6–8]. The effects of axial force on dynamic properties of various models of beams and multiple beam systems have also been studied extensively, and it has been shown that, as the axial force increases, the wave amplitudes increase as well, but the natural frequencies decrease [9, 10].

Thus, one of the most interesting and useful characteristics of phononic metamaterials is the potential to break the symmetry of wave propagation. Reciprocity of wave propagation is widely spread in nature and only under certain conditions, this reciprocity is broken with the consequence of one-way propagation or even complete wave attenuation [3]. Under most circumstances, the waves will propagate symmetrically between two points in space (the source and the receiver are interchangeable) [11]. In crystallography, this phenomenon occurs when the size of internal molecular structure is comparable to the wavelength of the propagating wave, which causes scattering of that wave (Bragg scattering) and results in different band structures [1, 4]. However, it has been discovered that these dispersion characteristics appear in macroscopic structures as well, due to periodicity in geometry, material properties or boundary conditions [2, 5, 7, 8, 12]. This imposed periodicity induces the opening of band gaps which appear when dispersion curves split, and disappear as soon as the periodicity is broken [2, 4]. Regardless of the studied medium, the position of band gaps depends upon unit cell size, which makes it difficult to achieve these dispersion characteristics for higher frequencies [2, 4]. There are many different scientifically proven ways to induce non-reciprocity, such as the implementation of local resonators [4], some of them are too complicated to be applied in reality, or cannot be applied, as new advances are needed in material engineering and fabrication [3]. A metamaterial can surely be created by modulating its spatial dimensions but this approach often has many limitations in terms of design and adaptability [13]. Thus, changing its material properties is a more universal and practical method. Various experiments have already been performed to demonstrate previously described phenomena.

It has been experimentally demonstrated that a beam modulated with piezoelectric actuators exhibit directional band gaps and unidirectional wave propagation and this type of bean has been used for waveguiding with the ability to select the output frequency [14, 15]. The same has been shown for elastic beams with

internal resonators which are able to dynamically modulate their stiffness in order to break the symmetry of wave propagation, with a very convenient ability to choose the appropriate frequency range [16]. The phenomenon of unidirectional wave propagation has also been proven in experiments with geometrical periodicity, i.e. on periodically undulated beams and plates and beams with periodically varying cross sections [17, 18]. Applications have been found in wave localization as well, by intentionally introducing a defect to the structure in a form of a specific pattern [4, 19].

In this paper, we have investigated a multiple-beam system with material layers in between. Three beams form a representative cell which is tessellated throughout the system, thus providing structural periodicity. Moreover, three different models of material layers have been explored. We have used the simplest linear elastic Winkler model, which does not provide any information concerning dissipation. Thus, a more complex two-parameter Pasternak model has been used in its elastic and viscoelastic form [20]. These layers also increase the stiffness of the system and account for vibration damping. In many studied cases in the available literature, only Winkler layer has been considered, but we have emphasized the model with Pasternak layers because the response of many materials which are used in engineering practice (i.e. rubber-like materials) cannot be approximated as purely elastic. Significant effects on the natural frequencies of the system have been shown when the shearing layer of the Pasternak elastic model is considered, as well as damping in the Pasternak viscoelastic model [21].

The main motivation behind this research work was to create a lattice made of slender beams with periodically changing interconnecting layers and structures, which can be incorporated in various structures and machines, in civil and mechanical engineering. Such structures can be used to gain similar effects of filtering and guiding of elastic waves which are present as disturbance or noise, especially when highly sensitive devices are concerned. The main advantage of this lattice model is that it is composed of multiple structural elements such as Euler–Bernoulli beams instead of interconnected point masses or single structural elements with modulated material or geometric properties. The tessellated cell which consists of three beams interconnected with layers differing in material properties can also be modified and expanded during application. Among all possible applications, we would like to highlight the fact that it is especially relevant for some structural problems encountered in civil engineering. Incorporating such models could provide elastic and acoustic cloaking, which can be crucial for protection from seismic waves and noise pollution [22, 23]. Here, all beams were loaded with time-varying axial forces. We induced periodicity with modulation of constitutive properties of material layers between the beams, as well as with modulation of beam stiffness through periodicity of axial forces acting on the beams. The general method for obtaining the dispersion relation for lattice structures with time-varying constitutive properties is presented in [24]. Along with the Floquet-Bloch theorem and Fourier expansion of stiffness and damping matrices, this method allows us to use the matrix differential equation of the system to obtain the dispersion relation in the form of a quadratic eigenvalue problem (QEP) [5, 24]. The effects of modulation can clearly

be seen on band diagrams, in which dispersion branches appear to "split". In this way, we discover frequencies at which unidirectional wave propagation appears and use this information to choose an excitation frequency that will produce such wave propagation. Thus, differential equations of motion can be solved with the provided excitation force for the middle beam in the system. We have applied the Galerkin method and found displacements of each beam using the finite difference method. Finally, we have plotted the resulting wave propagation and it can be seen that the wave propagates through the multiple beam structure, but there is no reciprocal wave propagation as symmetry has been broken. Additionally, we have shown the band diagrams and wave propagation for the case of the multiple beam system with Pasternak viscoelastic layers, when axial force is modulated, and the other system parameters remain constant.

2. Theoretical consideration of coupled beam phononics

2.1. Multiple Euler–Bernoulli system, interconnected with material layers. A system of simply supported Euler–Bernoulli beams is interconnected with material layers and loaded with axial forces, as can be seen in Fig. 1, where a system with Pasternak viscoelastic layers is presented. Apart from this model, Pasternak and Winkler's type elastic layers are considered. Further on, as we introduce each of these layers, it will be shown that they can be regarded as a special case of the Pasternak viscoelastic layer when some of its properties are factored out. The use of Euler–Bernoulli theory is justified, as we are considering thin beams loaded at low frequencies, which is to say that shear deformations and rotary inertia can be neglected [10]. A sequence of three beams (denoted with an ordinal number $r = 1, 2, 3$) are loaded with axial forces F_r. These three beams and corresponding layers form a cell that is tessellated throughout the system. The first beam in the cell is connected to the last beam of the previous cell and vice versa. Thus, a phononic system is formed, in which structural periodicity exists. The phononic structure of such multiple-beam system represents a problem which has been studied extensively in condensed matter physics and crystallography, from which the application of Floquet-Bloch theorem and use of band diagrams are repurposed for the sake of studying the structural dynamics of such mechanical systems [4]. This periodicity allows us to study one cell in order to obtain the dynamical properties of the system [4]. Furthermore, the axial forces are modulated as harmonic functions of time, with a different phase angle for each beam in the cell. This modulation provides for time-varying stiffness properties of the beam. The axial loads are varied in time in the following manner:

$$F_r(t) = F_0\Big[1 + \delta_m \cos\Big(\omega_m t + \frac{2\pi r}{3}\Big)\Big],$$

where F_0 is the reference intensity of axial forces, δ_m is the amplitude of modulation and ω_m is the circular frequency of modulation. We simultaneously modulate the material properties of connecting layers in the same way.

For the sake of brevity, the general equation of motion is defined for the middle beam in a cell, as it is only connected with the beams in the same cell. The

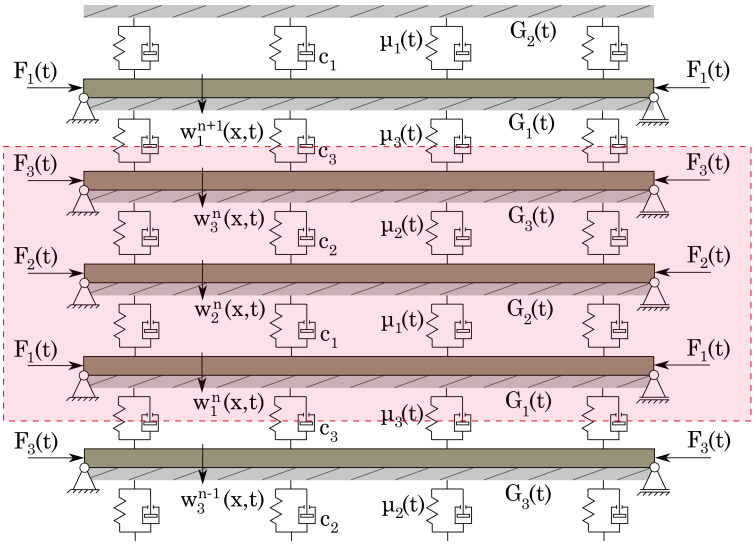

FIGURE 1. The schematic of a system of simply supported beams, interconnected with Pasternak viscoelastic layers. Three beams are grouped in a cell that is tessellated throughout the system (tinted window with a dashed outline).

constant elastic and inertial properties of the beam of length L are defined with Young's modulus E, density ρ, cross-sectional area A, and the area moment of inertia I. The dimensionless form of the partial differential equation of transverse motion for the middle beam in a cell is:

$$\frac{\partial^4 w_r}{\partial X^4} + \ddot{w}_r + F_r^*(\tau)\frac{\partial^2 w_r}{\partial X^2} + Q_r^*(\tau) = 0, \tag{2.1}$$

where w_r is the dimensionless transverse displacement of r^{th} beam in the cell. Dimensionless time and space coordinates have been introduced as $\tau = \Omega t$ $\left(\Omega = \frac{1}{L^2}\sqrt{\frac{EI}{\rho A}}\right)$ and $x = LX$. In this general equation, $Q_r^*(\tau)$ denotes the influence of surrounding material layers on the transverse motion of the beam (in dimensionless form), and $F_r^*(\tau)$ represents the dimensionless intensity of axial forces.

The governing differential equation for each beam in the cell is discretized by using the Galerkin method (presented in Appendix A) with an application of the Floquet-Bloch theorem. These discretized equations of motion are solved using the finite difference method (Appendix B).

2.2. Multiple Euler–Bernoulli beam system, connected with Pasternak viscoelastic layers (MBPV). We will investigate a multiple beam system with Pasternak viscoelastic layers (MBPV), which is depicted in Fig. 1. A Pasternak viscoelastic layer can be represented as a series of parallel springs and dashpots (viscous elements), connected to a viscous shearing layer [20]. The time-modulated

equivalent stiffness of springs is introduced as:

$$\mu_r(t) = \mu_0\Big[1 + \beta_m \cos\Big(\omega_m t + \frac{2\pi r}{3}\Big)\Big], \tag{2.2}$$

where μ_0 is the reference stiffness, β_m is the amplitude of modulation and ω_m is the circular frequency of modulation. The force resulting from the deformation of these layers can be calculated according to Hooke's law, as a linear function of displacements of the beams [20]. The equivalent damping of viscous elements for each layer is constant $c_r = c_0$, and the dissipative force is considered to be proportional to the rate of displacement [20].

Finally, the time-modulated coefficient of elastic resistance due to shearing deformations of the viscous shearing layer is:

$$G_r(t) = G_0\Big[1 + \gamma_m \cos\Big(\omega_m t + \frac{2\pi r}{3}\Big)\Big],$$

where G_0 is the reference coefficient and γ_m is the amplitude of modulation. The shearing forces (per unit length) are proportional to a mixed partial derivative of displacement, with respect to space and time [20].

According to the general form of the equation of motion (2.1), the resulting equations of motion for beams in one cell are:

$$\begin{aligned}
&\frac{\partial^4 w_1^n}{\partial X^4} + \ddot{w}_1^n + F_1^*(\tau)\frac{\partial^2 w_1^n}{\partial X^2} + \mu_1^*(\tau)(w_1^n - w_2^n) + \mu_3^*(\tau)(w_1^n - w_3^{n-1}) \\
&\qquad - G_1^*(\tau)\Big(\frac{\partial^2 w_1^n}{\partial X \partial \tau} - \frac{\partial^2 w_2^n}{\partial X \partial \tau}\Big) - G_3^*(\tau)\Big(\frac{\partial^2 w_1^n}{\partial X \partial \tau} - \frac{\partial^2 w_3^{n-1}}{\partial X \partial \tau}\Big) \\
&\qquad + c_1^*(\dot{w}_1^n - \dot{w}_2^n) + c_3^*(\dot{w}_1^n - \dot{w}_3^{n-1}) = 0,
\end{aligned} \tag{2.3}$$

$$\begin{aligned}
&\frac{\partial^4 w_2^n}{\partial X^4} + \ddot{w}_2^n + F_2^*(\tau)\frac{\partial^2 w_2^n}{\partial X^2} + \mu_2^*(\tau)(w_2^n - w_3^n) + \mu_1^*(\tau)(w_2^n - w_1^n) \\
&\qquad - G_2^*(\tau)\Big(\frac{\partial^2 w_2^n}{\partial X \partial \tau} - \frac{\partial^2 w_3^n}{\partial X \partial \tau}\Big) - G_1^*(\tau)\Big(\frac{\partial^2 w_2^n}{\partial X \partial \tau} - \frac{\partial^2 w_1^n}{\partial X \partial \tau}\Big) \\
&\qquad + c_2^*(\dot{w}_2^n - \dot{w}_3^n) + c_1^*(\dot{w}_2^n - \dot{w}_1^n) = 0,
\end{aligned}$$

$$\begin{aligned}
&\frac{\partial^4 w_3^n}{\partial X^4} + \ddot{w}_3^n + F_3^*(\tau)\frac{\partial^2 w_3^n}{\partial X^2} + \mu_3^*(\tau)(w_3^n - w_1^{n+1}) + \mu_2^*(\tau)(w_3^n - w_2^n) \\
&\qquad - G_3^*(\tau)\Big(\frac{\partial^2 w_3^n}{\partial X \partial \tau} - \frac{\partial^2 w_1^{n+1}}{\partial X \partial \tau}\Big) - G_2^*(\tau)\Big(\frac{\partial^2 w_3^n}{\partial X \partial \tau} - \frac{\partial^2 w_2^n}{\partial X \partial \tau}\Big) \\
&\qquad + c_3^*(\dot{w}_3^n - \dot{w}_1^{n+1}) + c_2^*(\dot{w}_3^n - \dot{w}_2^n) = 0,
\end{aligned} \tag{2.4}$$

where w_r is the dimensionless transverse displacement, $F_r^*(\tau)$ represents the dimensionless intensity of axial forces, μ_r^* is the dimensionless equivalent stiffness of springs, c_r^* is the dimensionless equivalent damping of dashpots and G_r^* is the dimensionless coefficient of elastic resistance of the viscous layer.

2.3. Multiple Euler–Bernoulli beam system, connected with Pasternak elastic layers (MBPE). Here, we will investigate a multiple beam system with Pasternak elastic layers (MBPE). These layers can be represented as a series of parallel springs which are connected to an elastic shearing layer [20], which is obtained when dashpots are removed from the system depicted in Fig. 1. The time-modulated equivalent stiffness of springs is introduced in the same manner, as it was done in Eq. (2.2). As for the elastic Pasternak layer, the time-modulated coefficient of elastic resistance due to shearing deformations is:

$$G_r(t) = G_0\Big[1 + \gamma_m \cos\Big(\omega_m t + \frac{2\pi r}{3}\Big)\Big],$$

where G_0 is the reference coefficient and γ_m is the amplitude of modulation. The shearing forces (per unit length) are proportional to the second space derivative of transverse displacement of the beam [20].

According to the general form of the equation of motion (2.1), the resulting equations of motion for the beams in one cell are:

$$\begin{aligned}(2.5)\qquad &\frac{\partial^4 w_1^n}{\partial X^4} + \ddot{w}_1^n + F_1^*(\tau)\frac{\partial^2 w_1^n}{\partial X^2} + \mu_1^*(\tau)(w_1^n - w_2^n) + \mu_3^*(\tau)(w_1^n - w_3^{n-1})\\ &\quad - G_1^*(\tau)\Big(\frac{\partial^2 w_1^n}{\partial X^2} - \frac{\partial^2 w_2^n}{\partial X^2}\Big) - G_3^*(\tau)\Big(\frac{\partial^2 w_1^n}{\partial X^2} - \frac{\partial^2 w_3^{n-1}}{\partial X^2}\Big) = 0,\end{aligned}$$

$$\begin{aligned}&\frac{\partial^4 w_2^n}{\partial X^4} + \ddot{w}_2^n + F_2^*(\tau)\frac{\partial^2 w_2^n}{\partial X^2} + \mu_2^*(\tau)(w_2^n - w_3^n) + \mu_1^*(\tau)(w_2^n - w_1^n)\\ &\quad - G_2^*(\tau)\Big(\frac{\partial^2 w_2^n}{\partial X^2} - \frac{\partial^2 w_3^n}{\partial X^2}\Big) - G_1^*(\tau)\Big(\frac{\partial^2 w_2^n}{\partial X^2} - \frac{\partial^2 w_1^n}{\partial X^2}\Big) = 0,\end{aligned}$$

$$\begin{aligned}(2.6)\qquad &\frac{\partial^4 w_3^n}{\partial X^4} + \ddot{w}_3^n + F_3^*(\tau)\frac{\partial^2 w_3^n}{\partial X^2} + \mu_3^*(\tau)(w_3^n - w_1^{n+1}) + \mu_2^*(\tau)(w_3^n - w_2^n)\\ &\quad - G_3^*(\tau)\Big(\frac{\partial^2 w_3^n}{\partial X^2} - \frac{\partial^2 w_1^{n+1}}{\partial X^2}\Big) - G_2^*(\tau)\Big(\frac{\partial^2 w_3^n}{\partial X^2} - \frac{\partial^2 w_2^n}{\partial X^2}\Big) = 0\end{aligned}$$

where G_r^* is the dimensionless coefficient of viscosity due to shear deformations [20].

2.4. Multiple Euler–Bernoulli beam system, connected with Winkler elastic layers (MBW). Here we will present a multiple beam system with Winkler elastic layers. These layers can be represented as a system of parallel linear springs with equivalent stiffness introduced in Eq. (2.2), which is depicted when the shearing layers and dashpots are removed from the system shown in Fig. 1. The resulting equations of motion for the beams in one cell are obtained when the forces resulting from the deformation of the shearing layer in Eqs. (2.5)–(2.6) are omitted, and they will not be given here, for the sake of brevity.

3. Application of Floquet–Bloch theorem

According to the Bloch theorem [4], we can express the relationship between displacements of two beams with the same ordinal number in adjacent cells:

$$w_j^{n-1} = e^{i\tilde{\mu}} w_j^n,$$

$$w_j^{n+1} = e^{-i\tilde{\mu}} w_j^n,$$

where $\tilde{\mu}$ is the dimensionless wave number expressed as a product of wave number κ and spatial wavelength of modulation λ_m.

After differential equations of motion are discretised according to Galerkin procedures discretized in Appendix A, we can now write the system of equations (2.3)–(2.4) in a condensed matrix form:

$$\mathbf{M}\ddot{\mathbf{q}}(\tau) + \mathbf{C}(\tau)\dot{\mathbf{q}}(\tau) + \mathbf{K}(\tau)\mathbf{q}(\tau) = 0, \tag{3.1}$$

where $\mathbf{M}$ is the mass matrix, $\mathbf{C}(\tau)$ is the stiffness matrix which is a function of dimensionless time, and $\mathbf{K}(\tau)$ is the damping matrix (also time-dependent). As there is no modulation of mass properties, the mass matrix is constant. For the case in which only axial forces are modulated, the damping matrix is constant, as well. These matrices are given in Appendix B. The displacement vector is denoted as $\mathbf{q}(\tau)$. Thus, the matrix equation (3.1) represents a system of $(N = 5 \times 3 = 15)$ differential equations, as there are five modes considered for displacements of each beam in the cell (containing three beams).

In order to describe the nature of wave propagation through the described system, we will derive the dispersion relation-the relationship between dimensionless frequency Ω and wavenumber μ. The solution for the displacement vector of the n-th cell is assumed according to the Bloch theorem [4, 5]:

$$\mathbf{q}_n(t) = e^{i(-n\tilde{\mu}+\omega t)} \sum_{p=-\infty}^{+\infty} e^{ip\omega_m t} \tag{3.2}$$

Furthermore, due to the periodic nature of modulation, stiffness and damping matrices can be expressed with Fourier series representation. However, it is convenient to transform these matrices to a sum of component matrices:

$$\mathbf{C}(t,\mu) = \mathbf{C}(t) + \mathbf{C}^{(l)}(t)e^{i\tilde{\mu}} + \mathbf{C}^{(r)}(t)e^{-i\tilde{\mu}}$$
$$\mathbf{K}(t,\mu) = \mathbf{K}(t) + \mathbf{K}^{(l)}(t)e^{i\tilde{\mu}} + \mathbf{K}^{(r)}(t)e^{-i\tilde{\mu}}$$

where superscripts l and r designate the fact that these are sparse matrices with the only non-zero element at the leftmost or rightmost diagonal. The Fourier expansion of component damping matrices is:

$$\mathbf{C}(t) = \sum_{k=-\infty}^{+\infty} \underset{\sim}{\mathbf{C}}_k(\tilde{\mu}) e^{ik\omega_m t},$$
$$\mathbf{C}^{(l)}(t) = \sum_{k=-\infty}^{+\infty} \underset{\sim}{\mathbf{C}}_k^{(l)}(\tilde{\mu}) e^{ik\omega_m t},$$
$$\mathbf{C}^{(r)}(t) = \sum_{k=-\infty}^{+\infty} \underset{\sim}{\mathbf{C}}_k^{(r)}(\tilde{\mu}) e^{ik\omega_m t}$$

where T_m is the temporal period of modulation. The ratio of spatial wavelength of modulation λ_m and temporal period of modulation gives the propagation velocity

of modulation wave $v_m = \frac{\lambda_m}{T_m}$. The temporal period of modulation is inversely proportional to the circular frequency of modulation $T_m = \frac{2\pi}{\omega_m}$. The Fourier expansion of component stiffness matrices $\mathbf{K}(t)$, $\mathbf{K}^{(l)}(t)$ and $\mathbf{K}^{(r)}(t)$ is analogous. Using the inverse Fourier transform we obtain:

$$\underset{\sim}{\mathbf{C}}_k^*(\tilde{\mu}) = \frac{1}{T_m}\int_{-\frac{T_m}{2}}^{\frac{T_m}{2}} \left[\mathbf{C}(t) + \mathbf{C}^{(l)}(t)e^{i\tilde{\mu}} + \mathbf{C}^{(r)}(t)e^{-i\tilde{\mu}}\right]e^{-ik\omega_m t}\mathrm{d}t$$

and

$$\underset{\sim}{\mathbf{K}}_k^*(\tilde{\mu}) = \frac{1}{T_m}\int_{-\frac{T_m}{2}}^{\frac{T_m}{2}} \left[\mathbf{K}(t) + \mathbf{K}^{(l)}(t)e^{i\tilde{\mu}} + \mathbf{K}^{(r)}(t)e^{-i\tilde{\mu}}\right]e^{-ik\omega_m t}\mathrm{d}t \tag{3.3}$$

When we introduce equations (3.2)–(3.3) to the equation of motion (3.1), we obtain the dispersion relation in a form of a quadratic eigenvalue problem (QEP):

$$\sum_{k=-\infty}^{+\infty}[\Omega + (p-k)\Omega_m]^2\mathbf{M} - i\sum_{k=-\infty}^{+\infty}[\Omega + (p-k)\Omega_m]\underset{\sim}{\mathbf{C}}_k^*(\tilde{\mu}) - \sum_{k=-\infty}^{+\infty}\underset{\sim}{\mathbf{K}}_k^*(\tilde{\mu}) = 0$$

where Ω_m is the dimensionless modulation frequency. When we let $k \in [-2, 2]$ and $p \in [-1, 1]$, $(P = 3)$, this QEP becomes:

$$\Omega^2\mathbf{Q}_A + \Omega\mathbf{Q}_B + \mathbf{Q}_C = 0 \tag{3.4}$$

where

$$\mathbf{Q}_A = \begin{bmatrix}\mathbf{M} & 0 & 0\\ 0 & \mathbf{M} & 0\\ 0 & 0 & \mathbf{M}\end{bmatrix}$$

$$\mathbf{Q}_B = 2\Omega_m\begin{bmatrix}-\mathbf{M} & 0 & 0\\ 0 & 0 & 0\\ 0 & 0 & \mathbf{M}\end{bmatrix} - i\begin{bmatrix}\underset{\sim}{\mathbf{C}}_0 & \underset{\sim}{\mathbf{C}}_{-1} & \underset{\sim}{\mathbf{C}}_{-2}\\ \underset{\sim}{\mathbf{C}}_1 & \underset{\sim}{\mathbf{C}}_0 & \underset{\sim}{\mathbf{C}}_{-1}\\ \underset{\sim}{\mathbf{C}}_2 & \underset{\sim}{\mathbf{C}}_1 & \underset{\sim}{\mathbf{C}}_0\end{bmatrix}$$

$$\mathbf{Q}_C = \Omega_m^2\begin{bmatrix}\mathbf{M} & 0 & 0\\ 0 & 0 & 0\\ 0 & 0 & \mathbf{M}\end{bmatrix} - \begin{bmatrix}\underset{\sim}{\mathbf{K}}_0 & \underset{\sim}{\mathbf{K}}_{-1} & \underset{\sim}{\mathbf{K}}_{-2}\\ \underset{\sim}{\mathbf{K}}_1 & \underset{\sim}{\mathbf{K}}_0 & \underset{\sim}{\mathbf{K}}_{-1}\\ \underset{\sim}{\mathbf{K}}_2 & \underset{\sim}{\mathbf{K}}_1 & \underset{\sim}{\mathbf{K}}_0\end{bmatrix} - i\Omega_m\begin{bmatrix}-\underset{\sim}{\mathbf{C}}_0 & 0 & \underset{\sim}{\mathbf{C}}_{-2}\\ -\underset{\sim}{\mathbf{C}}_1 & 0 & \underset{\sim}{\mathbf{C}}_{-1}\\ -\underset{\sim}{\mathbf{C}}_2 & 0 & \underset{\sim}{\mathbf{C}}_0\end{bmatrix}$$

Equation (3.4) represents a system of PxN=45 algebraic equations. As for the cases with Pasternak and Winkler elastic layers (MBPE and MBW), we obtain analogous equations and matrices, with the only difference being the absence of the damping matrix $\mathbf{C}$.

4. Numerical results

We have previously considered a multiple-beam system with three different types of material layers which provide coupling in the transverse direction of motion. The system is made by tessellation of a cell, which is composed of three beams and their accompanying layers. For simulation purposes, we investigated 50 cells with 3 beams in each cell. The beams were modeled according to the Euler–Bernoulli theory and three different types of layers were considered. Differential equations of motion were written for each beam in the cell and discretized according to the Galerkin method presented in Appendix A. During numerical calculations,

only the first five terms in the Galerkin approximation were adopted. As a result, we obtained a matrix differential equation of one variable $\mathbf{q}$, which is a time function vector of transverse displacement for each beam in a cell. The Floquet-Bloch theorem was used to obtain a condensed form of these equations (3.1) for MBPV, since there is coupling with surrounding cells. Then, we were able to produce an iterative equation suitable for further numerical calculations (B.2) for MBPV, using the finite difference method which was presented in Appendix B. Similar equations were obtained for MBPE and MBW when their characteristic properties were taken into consideration. The Floquet-Bloch theorem was also used to obtain the dispersion relation (3.4) in the form of a quadratic eigenvalue problem (QEP). It can be shown that Ω is a periodic function of μ, with period 2π. Thus, equation (3.4) can be solved when we let $\mu \in [-\pi, \pi]$, which is known as the First Brillouin Zone (FBZ) [5]. It can be seen that dispersion branches fold at the boundaries of the FBZ. This also allows us to discern directional band gaps, as both negative and positive directions of wave propagation are taken into consideration. The system parameters which were used during the calculation for MBPV are: $P_0 = 0.2$, $\mu_0 = 100$, $G_0 = 1$, $c_0 = 0.1$, $\Omega_m = 2$, $\delta_m = 0.1$, $\beta_m = 0.2$ and $\gamma_m = 0.1$. The parameters which are present in MBPE and MBW have the same values and will not be listed for the sake of brevity. The solution of the QEP is presented in the form of band diagrams from which we can subsequently choose the relevant excitation frequency. It should be noted that for each mode there are 3 families of dispersion branches, but only fundamental dispersion branches are shown in the dispersion analysis of the system. These branches are obtained by performing the weighting and threshold procedure [24], after which asymmetric directional band gaps are clearly visible. This procedure involves selecting the branch which corresponds to the fundamental plane wave (the one carrying the most energy), by identifying the eigenvector corresponding to the fundamental plane wave and using its values (the Euclidean norm) as a threshold to which all other values are compared, thus eliminating them from the final band diagram. The color legend given in each figure corresponds to the given values of the eigenvector. Directional band gap frequency ranges for the first mode of each case are given in Table 1. The chosen excitation frequencies Ω_{ex} are also presented in Table 1, and it can be seen that each excitation frequency corresponds to the highest frequency band gap of the first branch. In Figs. 2a–2c we have presented band gaps for the case of

TABLE 1. Band gaps boundaries in the first mode and chosen excitation frequencies for each considered case.

MBPV		MBPE		MBW	
band gap	Ω_{ex}	band gap	Ω_{ex}	band gap	Ω_{ex}
(12.39,13.08)		(12.95,13.67)		(12.61,13.32)	
(14.37,15.05)		(14.93,15,65)		(14.59,15.30)	
(17.96,19.44)		(18.76,20.26)		(18.03,19.51)	
(19.96,21.44)	20.5	(20.76,22.25)	21.5	(20.05,21.51)	20.8

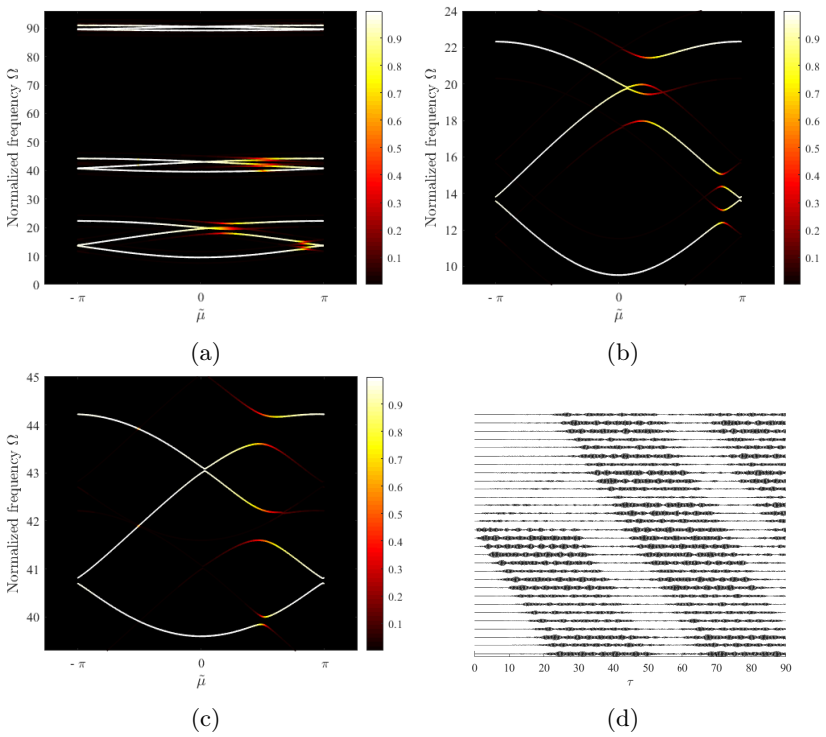

FIGURE 2. Dispersion and unidirectional wave propagation properties of the MBPV system: (a) fundamental dispersion branches for the first three modes, (b) fundamental dispersion branches for the first mode, (c) fundamental dispersion branches for the second mode, (d) unidirectional wave propagation for the excitation frequency $\Omega_{ex} = 20.5$.

MBPV, where axial forces and parameters of Pasternak viscoelastic layers (μ_r and G_r) were modulated in time. The band gaps for the case of MBPE are presented in Figs. 3a–3c, where the effects of time-modulated axial forces and parameters of Pasternak elastic layers (μ_r and G_r) can be seen. In Figs. 4a–4c we have presented band gaps for the case of MBW, where we have modulated axial forces and equivalent stiffness of springs. In Figs. 2a, 3a, and 4a we can see three sets of fundamental dispersion branches, corresponding to the first three modes. Figs. 2b, 3b and 4b show magnified fundamental dispersion branches related to the first mode, where the directional band gaps appear on the dispersion branch. In the case of MBW, these band gaps appear only for the positive wavenumbers in the branches related to the first two modes while there are no gaps in higher modes due to the damping effect (see Figs. 2a, 3a, and 4a). It should be noted that asymmetric gaps can appear in higher modes when lower damping values are adopted, but they will

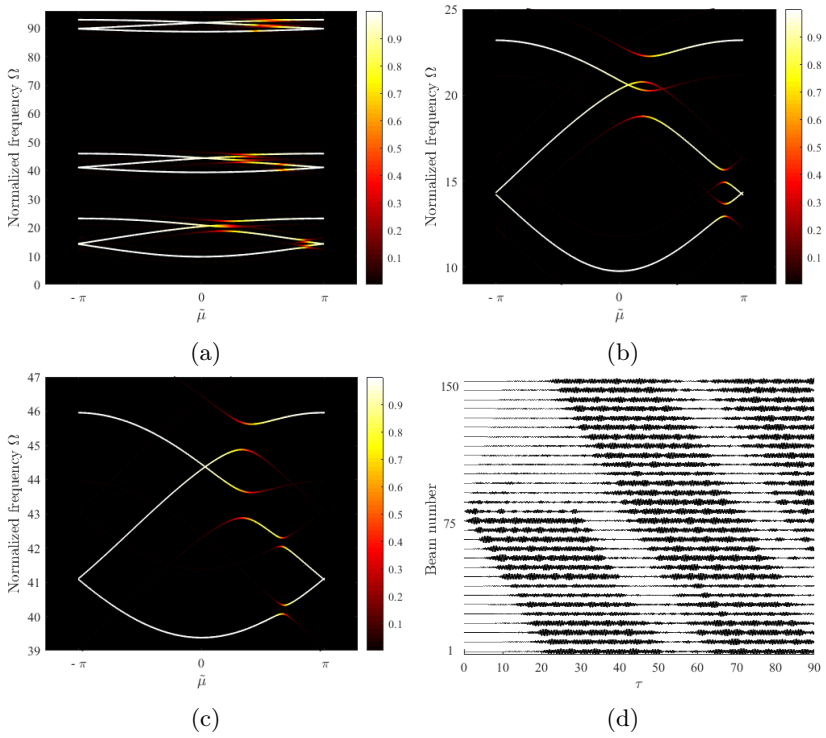

FIGURE 3. Dispersion and unidirectional wave propagation properties of the MBPE system: (a) fundamental dispersion branches for the first three modes, (b) fundamental dispersion branches for the first mode, (c) fundamental dispersion branches for the second mode, (d) unidirectional wave propagation for the excitation frequency $\Omega_{ex} = 21.5$.

be located in the negative half of the wavenumber axis. This analysis is omitted here for the sake of brevity. In the case of MBPE, all three modes have directional band gaps which appear only for positive wavenumbers. By comparing Fig. 3b and 2b, we can see that band gaps have slightly shrunk due to viscous damping. We can also note that with higher frequency, directional band gaps get wider. Unlike for the solitary Euler–Bernoulli beam, which was considered in [5], symmetry is broken and directional band gaps were achieved with time modulation of material properties in a multiple beam lattice which exhibits structural periodicity, without the need for space modulation.

In order to execute the simulation, an excitation load was applied to the beam in the middle of the system, in the form of a harmonic function of time with an amplitude of excitation $Q = 0.0001$. The excitation starts at the beginning of simulation and ends at $\tau_{ex} = 30$. The end of the entire simulation is at $\tau_s = 90$. The

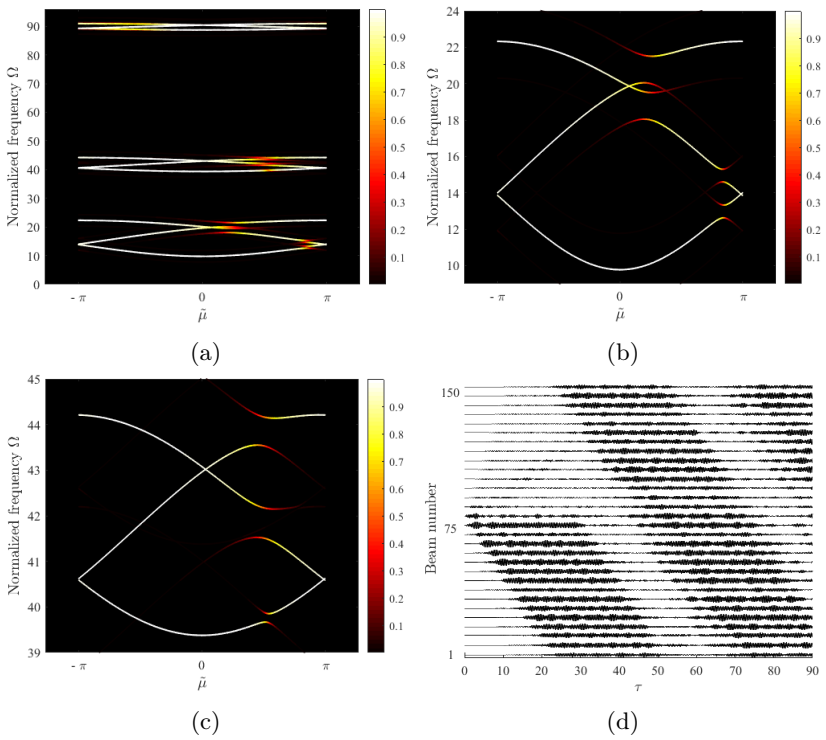

FIGURE 4. Dispersion and unidirectional wave propagation properties of the MBW system: (a) fundamental dispersion branches for the first three modes, (b) fundamental dispersion branches for the first mode, (c) fundamental dispersion branches for the second mode, (d) unidirectional wave propagation for the excitation frequency $\Omega_{ex} = 20.8$.

well-known convergence condition for the time step is $\Delta\tau \leqslant 10^{-3}$. For simulation purposes, we considered zero initial conditions ($\mathbf{q} = 0$, $\dot{\mathbf{q}} = 0$). The resulting wave propagation is presented in the form of a waterfall plot. Here, transverse displacements of beams were presented at the dimensionless space coordinate $X = 0.4$. We can see that, for each considered case (Figs. 2d, 3d and 4d), waves propagate through the system of beams, but only in the negative direction of the system. This indicates that the first mode has a negative group velocity. Since a finite system was considered in order to obtain numerical results, Born-Karman boundary conditions were imposed to prevent natural wave reflection at the end of the system. As a result, it can be seen that, once the end of the system is reached, the wave reappears at the other end of the system.

In the special case when only axial force is modulated, a comparatively high intensity of axial force is needed to achieve a band gap of considerable size in the

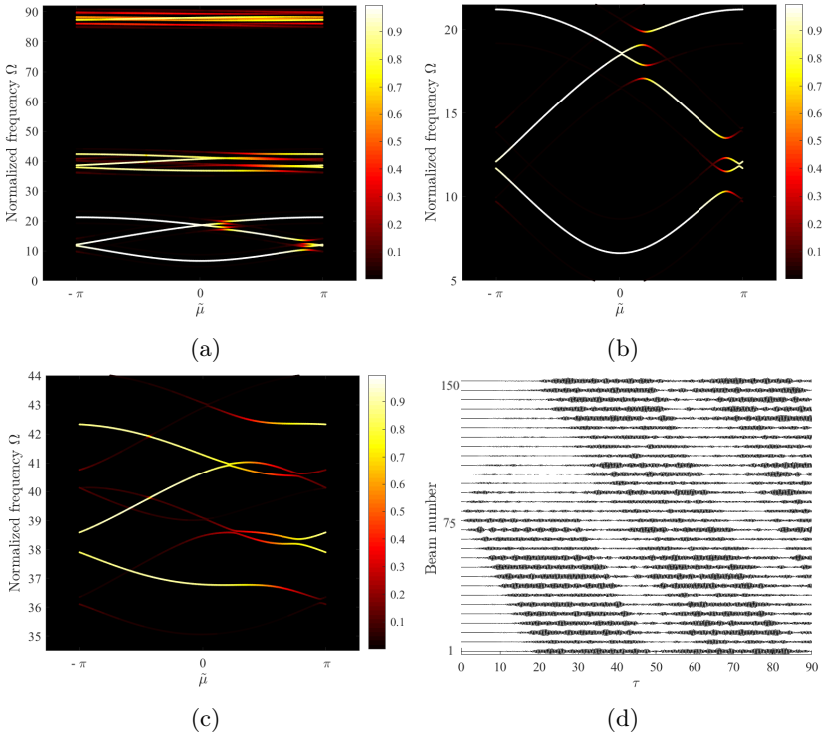

FIGURE 5. Dispersion and unidirectiona wave propagation properties of a system in which only the axial force acting on each beam is modulated: (a) fundamental dispersion branches for the first three modes, (b) fundamental dispersion branches for the first mode, (c) fundamental dispersion branches for the second mode, (d) unidirectiona wave propagation for the excitation frequency $\Omega_{ex} = 18.4$.

first mode, and the modulation frequency has to be higher as well, while the other system parameters remain constant. Here, the value which was used is $P = 5$ and the modulation frequency was $\delta_m = 0.6$. In Fig. 5a we can see band diagrams for the first three modes. In Figs. 5b and 5c the band diagrams for the first and second mode are presented, and directional band gaps are clearly visible. It should be noted that a significant decrease in frequency values is obvious, as these diagrams appear to have shifted downwards. Also, the band gaps are more narrow, and higher precision of excitation frequency is required to achieve uni-directional wave propagation. Here, the excitation frequency was $\Omega_{ex} = 19.4$, which corresponds to the highest frequency band gap in the first mode $\Omega \in (19.09, 19.88)$. The result is shown in Fig. 5d. One can also observe that in this case, most of the energy of wave motion is supported by waves that travel in one direction while some waves

with frequencies different from the main wave frequency are also excited and travel in both directions with group velocities different from the primary wave. The amplitude of these secondary waves is small compared to the primary wave.

Conclusions

We have analyzed a system of beams interconnected with three different material layers with time-varying axial loads and material properties. The beams were modeled according to Euler–Bernoulli beam theory. Such a system with periodically arranged beams represents a type of phononic structure which is researched in condensed matter physics. For each of these cases (differing in the ways in which the layers are modeled), we have obtained a band diagram by solving the eigenvalue problem, using Fourier series expansion and Floquet-Bloch theorem. As a result of parametric modulation, directional band gaps can clearly be recognized in these diagrams. Also, we have found the transient response of these systems, under harmonic transverse excitation load, which was continuously distributed. To this end, we have discretized partial differential equations of motion, which have subsequently been solved using the finite difference method. The results have been presented as waterfall plots in which unidirectional wave propagation can be seen. Thus, with time-varying properties of connecting layers, we can cause splitting in dispersion branches which leads to directional wave propagation in those frequency domains. In our future work, some of the main limitations of this model will be addressed, taking into consideration the fact that we have considered slender beams only, as well as the fact that these band gaps are quite narrow and some other modulation mechanisms should be explored to achieve wider band gaps.

Appendix A. Galerkin method

In order to discretize the governing equations of motion, we assume the solution according to the Galerkin method:

$$w_r(X,\tau) = \sum_{s=1}^{n} \phi_s(X) q_{s_r}(\tau) = \Phi(X)\mathbf{q}_r(\tau),$$

where s is the number of terms in the approximation. Throughout this paper, the number of adopted terms was 5. After discretization, we perform left-hand side multiplication with the transpose of Φ, and integrate over dimensionless space coordinate X. As a result of described Galerkin procedures and application of Floquet-Bloch theorem, we obtain the mass, stiffness and damping matrices, which, for the case with Pasternak viscoelastic layers, are:

$$\mathbf{M} = \begin{bmatrix} \mathbf{G}_A & 0 & 0 \\ 0 & \mathbf{G}_A & 0 \\ 0 & 0 & \mathbf{G}_A \end{bmatrix},$$

$$\mathbf{C}(\tau) = \begin{bmatrix} \mathbf{C}_{c_1} & G_1^*\mathbf{G}_D - c_1^*\mathbf{G}_A & (G_3^*\mathbf{G}_D - c_3^*\mathbf{G}_A)e^{i\tilde{\mu}} \\ G_1^*\mathbf{G}_D - c_1^*\mathbf{G}_A & \mathbf{C}_{c_2} & G_2^*\mathbf{G}_D - c_2^*\mathbf{G}_A \\ (G_3^*\mathbf{G}_D - c_3^*\mathbf{G}_A)e^{-i\tilde{\mu}} & G_2^*\mathbf{G}_D - c_2^*\mathbf{G}_A & \mathbf{C}_{c_3} \end{bmatrix},$$

where

$$\mathbf{C}_{c_r} = (c_r^* + c_{r-1}^*)\mathbf{G}_A - (G_r^* + G_{r-1}^*)\mathbf{G}_D$$

and

$$\mathbf{K}(\tau) = \begin{bmatrix} \mathbf{K}_{k_1} & -\mu_1^*\mathbf{G}_A & -\mu_3^*\mathbf{G}_A e^{i\tilde{\mu}} \\ -\mu_1^*\mathbf{G}_A & \mathbf{K}_{k_2} & -\mu_2^*\mathbf{G}_A \\ -\mu_3^*\mathbf{G}_A e^{-i\tilde{\mu}} & -\mu_2^*\mathbf{G}_A & \mathbf{K}_{k_3} \end{bmatrix}, \tag{A.1}$$

where

$$\mathbf{K}_{k_r} = \mathbf{G}_B + F_r^*\mathbf{G}_C + (\mu_r^* + \mu_{r-1}^*)\mathbf{G}_A.$$

where matrices $\mathbf{G}_A$, $\mathbf{G}_B$, $\mathbf{G}_C$ and $\mathbf{G}_D$ are:

$$\mathbf{G}_A = \int_0^1 \Phi^T(X)\Phi(X)\mathrm{d}X,$$
$$\mathbf{G}_B = \int_0^1 \Phi^T(X)\frac{\partial^4\Phi(X)}{\partial X^4}\mathrm{d}X,$$
$$\mathbf{G}_C = \int_0^1 \Phi^T(X)\frac{\partial^2\Phi(X)}{\partial X^2}\mathrm{d}X.$$
$$\mathbf{G}_D = \int_0^1 \Phi^T(X)\frac{\partial\Phi(X)}{\partial X}\mathrm{d}X.$$

When only the axial force is modulated, every Pasternak viscoelastic layer is the same throughout the system, with constant parameter values ($\mu_r = \mu_0$, $c_r = c_0$, $G_r = G_0$).

For the case with Winkler elastic layers, the stiffness matrix $\mathbf{K}$ appears in the same form (A.1), where $\mathbf{K}_{k_r} = \mathbf{G}_B + F_r^*\mathbf{G}_C + (\mu_r^* + \mu_{r-1}^*)\mathbf{G}_A$.

As for the case with Pasternak elastic layer, the stiffness matrix $\mathbf{K}$ appears in similar form:

$$\mathbf{K}(\tau) = \begin{bmatrix} \mathbf{K}_{k_1} & -\mu_1^*\mathbf{G}_A + G_1\mathbf{G}_C & (-\mu_3^*\mathbf{G}_A + G_3\mathbf{G}_C)e^{i\tilde{\mu}} \\ -\mu_1^*\mathbf{G}_A + G_1\mathbf{G}_C & \mathbf{K}_{k_2} & -\mu_2^*\mathbf{G}_A + G_2\mathbf{G}_C \\ (-\mu_3^*\mathbf{G}_A + G_3\mathbf{G}_C)e^{-i\tilde{\mu}} & -\mu_2^*\mathbf{G}_A + G_2\mathbf{G}_C & \mathbf{K}_{k_3} \end{bmatrix},$$

where

$$\mathbf{K}_{k_r} = \mathbf{G}_B + F_r^*\mathbf{G}_C + (\mu_r^* + \mu_{r-1}^*)\mathbf{G}_A - (G_r^* + G_{r-1}^*)\mathbf{G}_C.$$

Appendix B. Finite difference method

To find the solution, we have employed the finite difference method. The derivatives of displacement vector are approximated with the second order central difference:

$$\dot{\mathbf{q}} = \frac{\mathbf{q}^{i+1} - \mathbf{q}^{i-1}}{2\Delta\tau}$$
$$\ddot{\mathbf{q}} = \frac{\mathbf{q}^{i+1} - 2\mathbf{q}^{i} + \mathbf{q}^{i-1}}{\Delta\tau^2}$$

where superscripts are used to denote the time step (previous, current and following), i.e. $\mathbf{q}^{i+1} = \mathbf{q}(\tau + \Delta\tau)$.

After introducing this approximation to the equation (3.1), we obtain the following iterative solution:

$$\mathbf{q}^{i+1} = -\mathbf{M}^{-1}\underset{\sim}{\mathbf{P}}(\tau)\mathbf{q}^{i-1} - \mathbf{M}^{-1}\underset{\sim}{\mathbf{K}}(\tau)\mathbf{q}^{i} \tag{B.1}$$

where

$$\underset{\sim}{\mathbf{M}}(\tau) = \frac{\mathbf{M}}{\Delta\tau^2} + \frac{\mathbf{C}(\tau)}{2\Delta\tau},\ \underset{\sim}{\mathbf{P}}(\tau) = \frac{\mathbf{M}}{\Delta\tau^2} - \frac{\mathbf{C}(\tau)}{2\Delta\tau},\ \underset{\sim}{\mathbf{K}}(\tau) = \mathbf{K}(\tau) - \frac{2\mathbf{M}}{\Delta\tau^2}$$

When the excitation load is applied, the iterative equation B.1 becomes:

$$\mathbf{q}^{i+1} = -\underset{\sim}{\mathbf{M}}^{-1}\underset{\sim}{\mathbf{P}}\mathbf{q}^{i-1} - \underset{\sim}{\mathbf{M}}^{-1}\underset{\sim}{\mathbf{K}}\mathbf{q}^{i} + \underset{\sim}{\mathbf{M}}^{-1}\mathbf{f} \tag{B.2}$$

where $\mathbf{f}$ is the dimensionless transverse continuous load.

As for the systems with Pasternak elastic and Winkler elastic layers, in which the discretised differential equation has a similar form (without the damping matrix), the iterative solution is obtained analogously and will be omitted for the sake of brevity.

Acknowledgments

This research was supported by the Ministry of Education, Science and Technological Development of the Republic of Serbia through the Mathematical Institute SANU and Faculty of Mechanical Engineering, University of Belgrade (grant no. 451-03-68/2022-14/200105). This support is gratefully acknowledged.

References

1. A. Banerjee, R. Das, E. P. Calius, *Waves in structured mediums or metamaterials: A review*, Arch. Comput. Methods Eng. **26** (2019), 1029–1058.
2. Muhammad, C. W. Lim, *From photonic crystals to seismic metamaterials: A review via phononic crystals and acoustic metamaterials*, Arch. Comput. Methods Eng. **29** (2022), 1137–1198.
3. H. Nassar, B. Yousefzadeh, R. Fleury, M. Ruzzene, A. Alu, C. Daraio, A. N. Norris, G. Huang, M. R. Haberman, *Nonreciprocity in acoustic and elastic materials*, Nature Reviews Materials **5**(9) (2020), 667–685.
4. I. M. Hussein, J. M. Leamy, M. Ruzzene, *Dynamics of phononic materials and structures: Historical origins, recent progress, and future outlook*, Appl. Mech. Rev. **66**(4) (2014), 040802.
5. G. Trainiti, M. Ruzzene, *Non-reciprocal elastic wave propagation in spatiotemporal periodic structures*, New J. Phys. **18** (2016), 083047.
6. M. A. Attarzadeh, M. Nouh, *Non-reciprocal elastic wave propagation in 2D phononic membranes with spatiotemproally varying material properties*, J. Sound Vib. **422** (2018), 264–277.
7. E. Riva, M. Di Ronco, A. Elabd, G. Cazzulani, F. Braghin, *Non-reciprocal wave propagation in discretely modulated spatiotemporal plates*, J. Sound Vib. **471** (2020), 115186.
8. E. Riva, J. Marconi, G. Cazzulani, F. Braghin, *Generalized plane wave expansion method for non-reciprocal discretely modulated waveguides*, J. Sound Vib. **449** (2019), 172–181.
9. Y. Yesilce, *Effect of axial force on the free vibration of Reddy-Bickford multi-span beam carrying multiple spring-mass systems*, J. Vib. Control **16(1)** (2010), 11–32.
10. Y. Q. Zhang, Y. Lu, G. W. Ma, *Effect of compressive axial load on forced transverse vibrations of a double-beam system*, Int. J. Mech. Sci. **50** (2008), 299–305.
11. S. S. Rao, *Vibration of Continuous Systems*, John Wiley & Sons, Inc., 2007.
12. M. A. Attarzadeh, M. Nouh, *Non-reciprocal elastic wave propagation in 2D phononic membranes with spatiotemporally varying material properties*, J. Sound Vib. **422** (2018), 264–277.

13. Y. Wang, B. Yousefzadeh, H. Chen, H. Nassar, G. Huang, C. Daraio, *Observation of nonreciprocal wave propagation in a dynamic phononic lattice*, Phys. Rev. Lett. **121** (2018), 194301.
14. J. Marconi, E. Riva, M. Di Ronco, G. Cazzulani, F. Braghin, M. Ruzzene, *Experimental observation of nonreciprocal band gaps in a space-time-modulated beam using a shunted piezoelectric array*, Physical Review Applied **13** (2020), 031001.
15. G. Trainiti, Y. Xia, J. Marconi, G. Cazzulani, A. Erturk, M. Ruzzene, *Time-periodic stiffness modulation in elastic metamaterials for selective wave filtering: Theory and experiment*, Phys. Rev. Lett. **122** (2019), 124301.
16. M. A. Attarzadeh, J. Callanan, M. Nouh, *Experimental observation of nonreciprocal waves in a resonant metamaterial beam*, Physical Review Applied **13** (2020), 021001.
17. G. Trainiti, J. J. Rimoli, M. Ruzzene, *Wave propagation in periodically undulated beams and plates*, Int. J. Solids Struct. **75–76** (2015), 260–276.
18. F. Gao, Z. Wu, F. Li, C. Zhang, *Numerical and experimental analysis of the vibration and band-gap properties of elastic beams with periodically variable cross sections*, Waves Random Complex Media **29** (2019), 299–316.
19. R. L. Thomes, D. Beli, C. J. De Marqui, *Space-time wace localization in electromechanical metamaterial beams with programmable defects*, Mech. Syst. Signal Process. **167** (2022), 108550.
20. D. Younesian, A. Hosseinkhani, H. Askari, E. Esmailzadeh, *Elastic and viscoelastic foundations: a review on linear and nonlinear vibration modeling and applications*, Nonlinear Dyn. **97** (2019), 853–895.
21. T. M. Wang, J. E. Stephens, *Natural frequencies of Timoshenko beams on pasternak foundations*, J. Sound Vib. **51**(2) (1977) 149–155.
22. S. A. Cummer, J. Christensen, A. Alu, *Controlling sound with acoustic metamaterials*, Nature Reviews Materials **1**(3) (2016), 16001.
23. K. H. Madine, J. D. Colquitt, *Negative refraction and mode trapping of flexural-torsional waves in elastic lattices*, Philos. Trans. R. Soc. Lond., A, Math. Phys. Eng. Sci. **380** (2022), 20210379.
24. J. Vila, R. K. Pal, M. Ruzzene, G. Trainiti, *A bloch-based procedure for dispersion analysis of lattices with periodic time-varying properties*, J. Sound Vib. **406** (2017) 363–377.

ЈЕДНОСМЕРНА ПРОПАГАЦИЈА ТАЛАСА ПРИ ПАРАМЕТАРСКОЈ МОДУЛАЦИЈИ ФОНОНСКИХ СТРУКТУРА САСТОЈАНИХ ОД ВИТКИХ ГРЕДА

Резиме. Филтрирање, спровођење и слабљење таласа је актуелна тема научних истраживања, с обзиром на то да постоји велики простор за побољшање постојећих решења у модерној индустрији. Један од скорашњих напредака је остварен коришћењем нереципрочних метаматеријала. Метаматеријали имају неке особине због којих су се показали као врло погодни за примену у разним областима инжењерства. У овом раду, проучавамо нереципрочно простирање таласа у фононским структурама међусобно спрегнутих витких греда, до кога долази због модулације аксијалног оптерећења и параметара којима су представљене особине материјала. Упоредили смо резултате који су добијени за греде међусобно повезане Винклеровим еластичним слојевима, као и еластичним и вискоеластичним Пастернаковим слојевима. Дисперзиона анализа и простирање таласа кроз такве системе греда, при одговарајућим фреквенцијама побуде, извршени су аналитичким путем. Предложени приступ може се користити у анализи фононских структура сачињених од греда које су повезане на различите начине, као и греда које се могу описати помоћу теорија вишег реда.

Faculty of Mechanical Engineering
University of Belgrade
Belgrade
Serbia

Department of Mechanics
Mathematical Institute of the SASA
Belgrade
Serbia
danilok@mi.sanu.ac.rs

Department of Mechanics
Mathematical Institute of the SASA
Belgrade
Serbia

Faculty of Mechanical Engineering
University of Belgrade
Belgrade
Serbia

(Received 30.11.2022)
(Revised 06.12.2022)
(Available online 14.12.2022)